

Defect Creation in Surface-Mounted Metal–Organic Framework Thin Films

Zheng Wang,[†] Sebastian Henke,[§] Michael Paulus,^{||} Alexander Welle,[⊥] Zhiying Fan,[†] Katia Rodewald,[‡] Bernhard Rieger,[‡] and Roland A. Fischer^{*,†}

[†]Chair of Inorganic and Metal Organic Chemistry, Department Chemistry & Catalysis Research Center and [‡]WACKER Chair of Macromolecular Chemistry, Department Chemistry & Catalysis Research Center, Technical University of Munich (TUM), Lichtenbergstr. 4, 85748 Garching, Germany

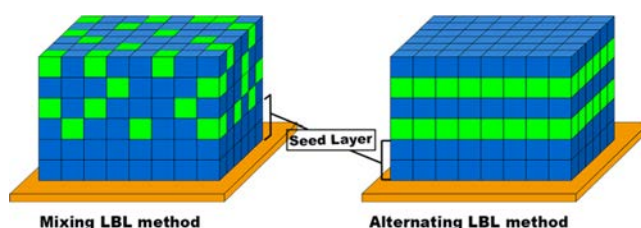
[§]Anorganische Chemie, Fakultät für Chemie und Chemische Biologie, Technische Universität Dortmund, Otto Hahn Str. 6, 44227 Dortmund, Germany

^{||}Fakultät Physik/DELTA, Technische Universität Dortmund, Maria Goeppert Mayer Str. 2, 44221 Dortmund, Germany

[⊥]Karlsruher Institut für Technologie, Institut für Funktionelle Grenzflächen (IFG) and Karlsruhe Nano Micro Facility (KNMF), Hermann von Helmholtz Platz 1, 76344 Eggenstein Leopoldshafen, Germany

ABSTRACT: Defect engineering is a strategy for tailoring the properties of metal–organic frameworks (MOFs). Plenty of efforts have been devoted to study the defect chemistry and structures of bulk MOFs; however, the reported example of a defect engineered surface mounted MOF (SURMOF) thin film is rare. In this work, defects were incorporated in SURMOF thin films by using defect generating linkers and taking advantage of the liquid phase stepwise epitaxial layer by layer growth (LBL). Two methods based on the LBL, named mixing method and alternating method, are proposed for incorporating defects in the prototypical SURMOF HKUST 1 by partially substituting the parent H₃btc (benzene 1,3,5 tricarboxylic acid) linker with a set of defect generating linkers H₂ip (isophthalic acid), H₂OH ip (5 hydroxyisophthalic acid), and H₂pydc (3,5 pyridinedicarboxylic acid). The crystallinity and phase purity of the obtained “defected” SURMOFs were confirmed by X ray diffraction, infrared reflection absorption spectroscopy, and Raman spectroscopy. The incorporation of the defect generating linkers and the types of induced defects were characterized by ultraviolet–visible spectroscopy, time of flight secondary ion mass spectrometry, methanol adsorption, scanning electron microscopy, and ¹H nuclear magnetic resonance spectroscopy (after digestion of the samples). These two methods provide avenues for controlling the defect formation in MOF thin films.

KEYWORDS: defect engineering, SURMOF, HKUST 1, thin films, UV–vis, defective linkers



1. INTRODUCTION

Metal–organic frameworks (MOFs) are a class of crystalline microporous materials with large internal surface areas, controlled porosities, and tunable properties,^{1–3} which show great potential in many application fields like storage,⁴ separation,⁵ catalysis,⁶ and chemical sensing.⁷ However, many challenges need to be solved for MOFs before stepping into real world technologies. Among them, the issues related to improving the performances of parent MOFs, for example, by implementing multifunctionalities and integrating into devices, are of great importance.⁸ Especially aiming for sustainable technology development, this demand is more urgent. Up to now, many synthetic strategies have been proposed to endow MOFs with multifunctionalities.^{9–16} One of these strategies is defect engineering, which creates metal and/or linker vacancies in MOFs by partially substituting the parent linker with a so called defective linker.¹¹ The presence of metal and linker vacancies may enhance the functional properties of MOFs,

such as porosity,¹⁷ catalytic activity,¹⁸ and magnetic behavior,¹⁹ or even creates new properties, such as charge transport.²⁰ Most recently, defect engineered MOF films are also reported for many applications. For instance, defect engineered ZIF 8 films synthesized by partially substituting parent linkers with defective linkers show advanced gas separation and carbon capture properties.^{21–25} The redox conductivity and electro catalytic activity of UIO 66 films can be tuned via control of the defect density in the framework.²⁶

Defects can be formed in MOFs intentionally by de novo synthesis²⁷ and special post synthetic treatment;²⁸ meanwhile, they may also be present inherently.²⁹ It is still a great challenge to control the formation of defects in MOFs (e.g., type, quantity, and distribution), which is important for many

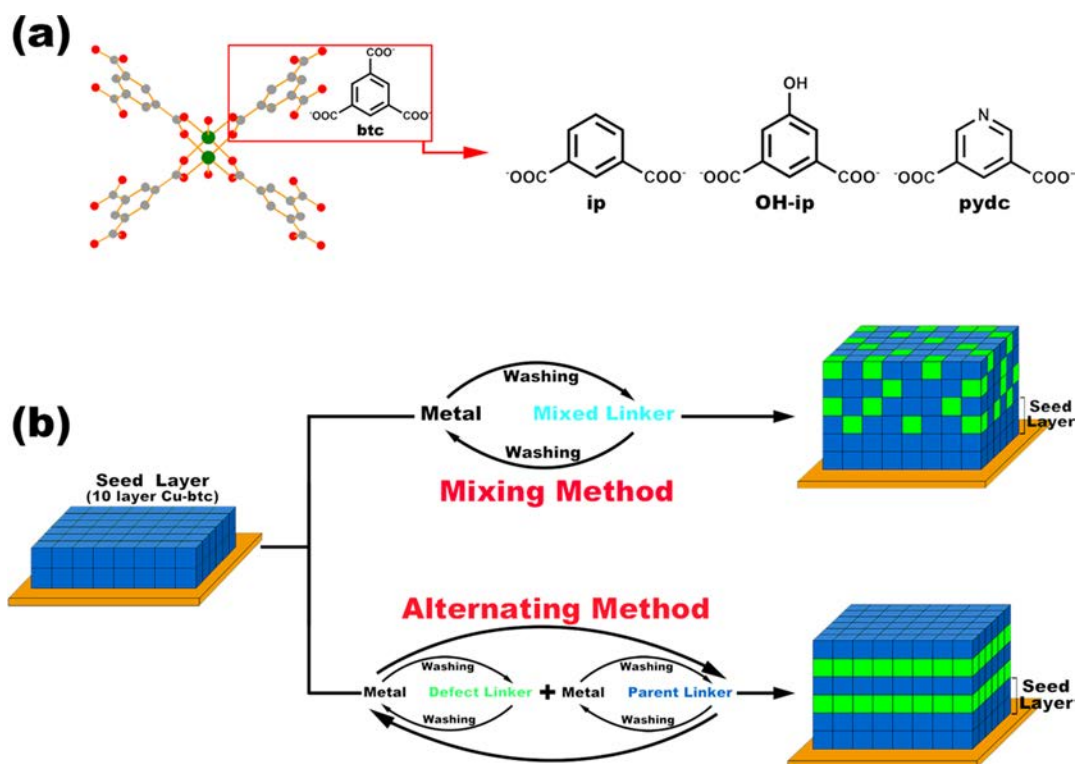


Figure 1. Schematic illustration of (a) DE SURMOFs HKUST 1 formed by partially substituting the parent H_3 btc linker with defective linkers H_2 ip, H_2 OH ip, and H_2 pydc; (b) the two methods for incorporating defects in SURMOF HKUST 1: the mixing method and alternating method.

fundamental studies. Moreover, the degree of defect incorporation may affect the structural integrity; and as more defects are present, the material will become more and more instable. For instance, defect engineered HKUST 1 (also known as Cu_3 btc $_2$, btc = benzene 1,3,5 tricarboxylate) can only incorporate the defective linker of ip (isophthalate) up to 50% of the feeding amount under solvothermal conditions, and beyond this threshold, the HKUST 1 structure type will not be formed.^{30,31}

To date, the most synthetic efforts have been devoted to bulk MOF materials;^{30,32} nevertheless, limited numbers of defect engineered MOF thin films have been reported, especially the surface mounted MOF (SURMOF) thin films.^{21–26,33,34} Herein, we try to incorporate defects in SURMOFs by taking advantage of the stepwise liquid phase epitaxial layer by layer (LBL) technique.^{13,35,36} LBL is a promising technique for fabricating MOF thin films due to its high controllability of the growth process.³⁷ Typically, the metal and linker are dosed on the functionalized substrate in a sequential fashion with rinsing after each step to remove the unreacted or physisorbed species. Moreover, in combination with surface plasmon resonance techniques³⁶ and quartz crystal microgravimetry (QCM),³⁸ the LBL growth process can be monitored in situ. The oscillation frequency change of the QCM sensor during the thin film growth process is recorded, and the resolution in terms of mass sensitivity is a few nanograms. The concept of this work is utilizing the LBL technique to synthesize defect engineered SURMOFs (DE SURMOFs). Compared to other film growth methods (e.g., solvothermal growth), the LBL technique shows high controllability of the growth process and also provides a closer inspection of defect incorporation in the MOF lattice.

Moreover, the LBL derived SURMOFs typically show controllable thickness and preferred orientation.^{15,37}

In this work, we report our investigations on DE SURMOFs of the HKUST 1 structure type. Thin film synthesis is performed by partially substituting the parent H_3 btc linker with a set of defect generating linkers H_2 ip, H_2 OH ip (5 hydroxyisophthalic acid), and H_2 pydc (3,5 pyridinedicarboxylic acid) using the LBL technique (Figure 1a). We investigate two different methods for creating defects in SURMOF HKUST 1 (Figure 1b): (1) mixing method, imitating the de novo synthesis of bulk MOFs, in which the linker solution used in the growth process is the mixture of parent and defective linkers;¹⁹ (2) alternating method, in which the substrate is separately exposed to parent linker solution and defective linker solution in an alternating way. The obtained DE SURMOFs HKUST 1 were characterized by X ray diffraction (XRD), infrared reflection absorption spectroscopy (IRRAS), and Raman spectroscopy to confirm that the structure of HKUST 1 does not change by incorporating defective linkers into the lattice. The combination of time of flight secondary ion mass spectrometry (ToF SIMS), ultraviolet–visible spectroscopy (UV–vis), methanol adsorption, and scanning electron microscopy (SEM) together with of 1H NMR after digestion of the DE SURMOF samples allowed the characterization of the defects incorporated in the framework of HKUST 1. Finally, the two methods of defect creation in SURMOF HKUST 1 are discussed and compared.

2. EXPERIMENTAL DETAILS

2.1. Materials. The chemicals ethanol (99.96%, VWR), Cu (OAc) $_2$ (98+%, Alfa Aesar), H_3 btc (98%, abcr), H_2 ip (99%, Sigma Aldrich), H_2 OH ip (98%, Alfa Aesar), and H_2 pydc (98%, Acros) are commercially available and were used as received without further purification.

2.2. General Methods. The crystallinity and orientation of the obtained SURMOFs were identified by grazing incidence X ray diffraction (GIXRD, Panalytical Empyrean instrument, grazing incidence mode, room temperature, Cu K α radiation, the range of $2\theta = 5-18^\circ$, a step of 0.01313° , accumulation time of 1.5 s per step) and 2D GIXRD (Beamline 9 of DELTA Dortmund, Germany, monochromatic X ray beam with an energy of 13 keV and a wavelength of 0.9607 \AA , room temperature, MAR 345 detector, sample to detector distance of 354.37 mm). IRRAS measurements were performed on a Bio Rad Excalibur FTIR spectrometer (FTS 3000) with 2 cm^{-1} resolution at an angle of incidence of 80° relative to the surface normal and further processed by using boxcar apodization. Raman spectra were recorded using a Renishaw Raman microscope spectrometer with an Ar⁺ laser emitting at 785 nm, output power limited to 10% (100% power is 300 mW). ¹H NMR spectroscopy was recorded at room temperature on a Bruker AV400 spectrometer, and the signal was referenced to that of DMSO d_6 . ToF SIMS was performed on a TOF.SIMS 5 instrument (ION TOF GmbH, Münster, Germany). UV-vis spectroscopy measurements were performed on a SHIMADZU UV 3600 Plus UV-vis-NIR spectrophotometer. SEM images were taken with a JEOL JSM 7500F field emission scanning electron microscope under gentle beam mode. Methanol adsorption of the SURMOFs was measured by an environment controlled quartz crystal microbalance (BEL QCM instrument, BEL Japan). Prior to sorption measurements, the SURMOFs were activated by soaking in pure CH₂Cl₂ for 2 days at room temperature and subsequently dried in a pure N₂ stream. Additionally, the samples were placed into the BEL QCM instrument cells at 25 °C under He stream (99.999%, 100 sccm) for about 4 h. After the activation process, the QCM frequency was recorded when the frequency change was stable within $\pm 5 \text{ Hz}$ over 30 min. Afterward, methanol sorption isotherms were collected by varying the relative vapor pressure (P/P_0) of saturated vapor of methanol molecules in a He gas stream at 25 °C ranging from 0 to 95.0%. The mass of the SURMOFs and adsorption amounts were calculated from the difference of the read QCM frequency and the fundamental frequency of the bare QCM substrate according to Sauerbrey's equation.

2.3. Pretreatment of QCM Substrates. The Au coated QCM substrates (AT cut type, Au electrode, diameter of 14 mm, thickness of 0.3 mm, and fundamental frequency of $\sim 4.95 \text{ MHz}$) were used for thin film growth. Prior to the film growth, QCM substrates were cleaned by immersing in a solution of water/H₂O₂/ammonia with a volume ratio of 5:1:1 at 75 °C for 15 min. Thereafter, the cleaned QCM substrates were functionalized by immersing in a 20 μM self assembly monolayer (SAM) solution of 16 mercaptohexadecanoic acid (MHDA) in ethanol for 1 day under room temperature followed by rinsing with pure ethanol.

2.4. Thin Films Grown by the Mixing Method. 0.2 mM linker solution was prepared by dissolving parent and defective linkers (molar ratio 1:1) in a mixed solvent of water/ethanol ($v/v = 2/8$). Meanwhile, the Cu(OAc)₂ solution was prepared using pure ethanol. SURMOFs were fabricated by LBL using the automated QCM instrument Q Sense E4 Auto at 40 °C with a flow rate of 100 $\mu\text{L}/\text{min}$. First, 10 cycles of HKUST 1 thin films were deposited on the SAM functionalized QCM substrate as the seed layer, and then another 50 cycles of the Cu(OAc)₂/mixed linker were subsequently deposited. In each deposition cycle, the QCM substrate was first exposed to 0.5 mM Cu(OAc)₂ solution for 5 min and then 0.2 mM linker solution for 10 min. Each subsequent step of dosing components was separated by a washing step with absolute ethanol for 5 min.

2.5. Thin Films Grown by the Alternating Method. SURMOFs were synthesized by the following procedure: (1) 10 cycles of HKUST 1; (2) Cu(OAc)₂/ethanol/defective linker/ethanol; and (3) Cu(OAc)₂/ethanol/parent linker/ethanol. The time of each cycle is the same as above. The last two steps were repeated 25 times for obtaining thick films. The concentrations of Cu(OAc)₂, parent linker, and defect linker were 0.5, 0.2, and 0.2 mM, respectively. The same mixed solvent (water/ethanol = 2/8) was used as the solvent for the linkers.

3. RESULTS AND DISCUSSION

3.1. Growth of DE-SURMOFs HKUST-1. The DE SURMOFs HKUST 1 in this work were fabricated by using the LBL technique. The growth process of SURMOF can be followed by the frequency change against time ($\Delta F - t$) curve recorded by QCM. For clarity, the samples prepared by the mixing method and alternating method using the ip defective linker are denoted as ip M and ip A (OH ip and pydc are denoted accordingly), respectively.

3.1.1. Mixing Method. In this method, the parent and defective linkers are blended with a 1:1 molar ratio as the linker solution for fabricating DE SURMOFs. The mass deposition on the substrate can be followed by the $\Delta F - t$ growth curves (left panels in Figure S1, Supporting Information). The zoom in (right panels of Figure S1) reveals that the defective linkers show diverse levels of incorporation or framework doping ($\text{H}_2\text{ip} < \text{H}_2\text{OH ip} < \text{H}_2\text{pydc}$) in SURMOF HKUST 1, which leads to different mass depositions of the DE SURMOF growth cycles, while the seed layer growth cycles, obviously, have similar mass deposition.

3.1.2. Alternating Method. In the method, the parent linker solution and defective linker solution are independently dosed on the substrate in an alternating way. In a typical growth procedure, 10 cycles of seed HKUST 1 were deposited first as the seed layer, and then the loop of 1 cycle of Cu(OAc)₂/H₃btc followed by 1 cycle of the Cu(OAc)₂/defective linker (ABAB fashion) was repeated 25 times to obtain DE SURMOF HKUST 1. The $\Delta F - t$ growth data shown in Figure S2 indicate the growth of MOF thin films. Similar to the mixing method, the diverse framework doping of defective linkers leads to different deposited masses of the Cu(OAc)₂/defective linker in the dosing cycles (right column of Figure S2). Moreover, the total frequency change or mass deposition of DE SURMOFs fabricated by the alternating method is less than those synthesized by the mixing method.

3.2. Phase Confirmation of DE-SURMOFs HKSUT-1. The purpose of introducing defects into SURMOFs is modifying the intrinsic properties of MOFs without changing the overall structure. Herein, the obtained DE SURMOFs HKUST 1 were at first characterized by XRD, IRRAS, and Raman spectroscopy to confirm their structures.

3.2.1. XRD Patterns. The out of plane XRD patterns are presented in Figure 2, from which we can see that the diffraction peaks of DE SURMOFs are assigned to the

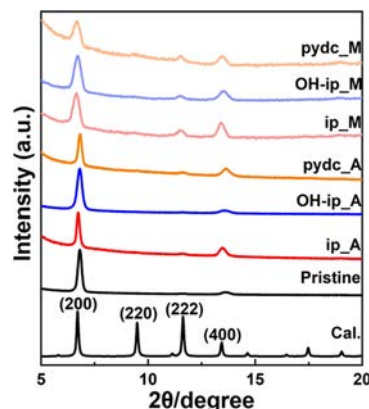


Figure 2. XRD patterns of DE SURMOFs HKUST 1 fabricated by the mixing method (light color) and alternating method (deep color).

HKUST 1 phase and the obtained thin films show a preferred orientation along the (100). By comparison of the characteristic XRD peaks, we find that DE SURMOFs fabricated via the mixing method show broader peaks than those prepared via the alternating method. This observation indicates a smaller crystallite size and overall poorer crystallinity of the thin films prepared via the mixing method, possibly due to an increased defect density.³⁹ Supplementary 2D GIXRD patterns (inclusive in plane and out of plane diffraction data) of the thin films synthesized by the alternating method further evidence the strongly preferred orientation of the HKUST 1 phase and the absence of any impurity phases as a consequence of defect linker incorporation (Figure S3). Moreover, the deposition of pure HKUST 1 as the seed layer has a significant impact on the crystallinity of the DE SURMOFs. As we can see in Figure S4, the presence of a seed layer greatly promotes the crystallinity and crystallographic orientation of the DE SURMOFs HKUST 1.

3.2.2. IRRAS and Raman Spectra. The IRRAS and Raman spectra are shown in Figure 3 and Figure S5, respectively. For

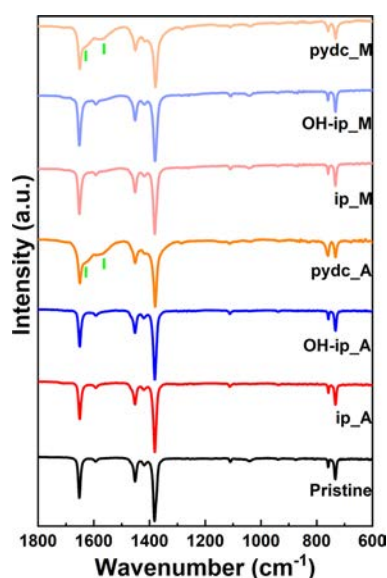


Figure 3. IRRAS spectra of pristine (black) and DE SURMOF HKUST 1 fabricated by the mixing method (light color) and alternating method (deep color). Herein, the peaks located at 1631 and 1572 cm^{-1} indicated by green tick marks are the COO^- vibration originating from mixed $[\text{Cu}_2(\text{btc}/\text{pydc})_n(\text{OAc})_{4-n}]$ paddlewheels and $[\text{Cu}_2(\text{OAc})_4]$ paddlewheels, respectively.

those DE SURMOFs HKUST 1 doped with ip and OH ip, the IRRAS and Raman spectra agree well with those of pristine HKUST 1. However, two additional peaks located at 1631 and 1572 cm^{-1} , indicated by green tick marks, are observed in the IRRAS spectra of **pydc M** and **pydc A**, which are assigned to the COO^- vibration originating from mixed $[\text{Cu}_2(\text{btc}/\text{pydc})_n(\text{OAc})_{4-n}]$ paddlewheels and $[\text{Cu}_2(\text{OAc})_4]$ paddlewheels, respectively.⁴⁰ The presence of mixed $[\text{Cu}_2(\text{btc}/\text{pydc})_n(\text{OAc})_{4-n}]$ paddlewheels in the framework demonstrates that acetate groups act as the counter anions in the modified paddlewheels (Figure 4a).³⁰ Meanwhile, the observation of the vibrational bands for $[\text{Cu}_2(\text{OAc})_4]$ paddlewheels suggests that a substantial amount of copper(II) acetate precursor is included in the pores of SURMOF HKUST 1, probably due to binding of the pyridinic N of pydc to the copper(II) acetate

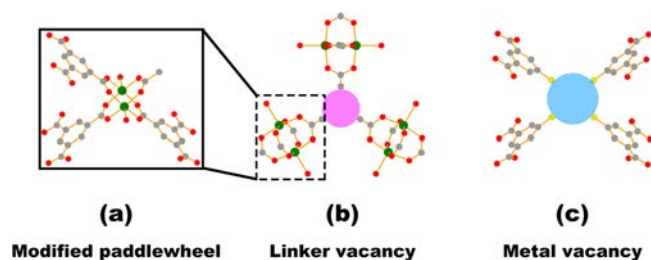


Figure 4. (a) Modified paddlewheel, (b) linker vacancy, and (c) metal vacancy.

paddlewheels. In accordance with the IRRAS spectra, additional bands originating from such acetate based paddlewheels are also observed by Raman spectroscopy (Figure S5).⁴¹ The absence of these two bands in the ip and OH ip defected DE SURMOFs HKUST 1 is probably because of their lower doping levels.

Based on the results and discussions above, it is concluded that the incorporation of defects in SURMOFs HKUST 1 does not change the overall network topology, at least at the studied levels of defect linker doping. Moreover, we deduced the possible defect types in DE SURMOFs HKUST 1 based on the data, which are shown in Figure 4 in accordance to the previously studied bulk samples of DE HKUST 1.³⁰

3.3. Defect Characterization in DE-SURMOF HKUST-1.

The incorporation of defective linkers in MOFs can generate metal and linker vacancies, both of which are important for tailoring the properties of MOFs.⁴² However, it is still a challenge to detect these defects in MOFs.⁴³ For bulk defect engineered HKUST 1, a vital characterization for defects is the determination of Cu^+ ions in the framework,^{19,30} while limited Cu^+ ions were formed in the growth process of SURMOF HKUST 1 due to the Cu^{2+} source used and the mild synthetic conditions. In this work, we characterize the defects in DE SURMOFs by mainly focusing on the identification of framework incorporated defective linkers (^1H NMR spectroscopy, ToF SIMS, and UV-vis spectra) and also by analyzing the porosity (methanol adsorption isotherms) and the thin film morphology (SEM).

3.3.1. Quantitative Detection of Defective Linkers in DE-SURMOFs (^1H NMR and TOF-SIMS). The incorporated defective linkers in DE SURMOFs HKUST 1 were quantitatively detected by ^1H NMR spectroscopy after digesting thin films in a mixture of DMSO d_6 and deuterium chloride in deuterated water ($\text{DCl}/\text{D}_2\text{O}$). Results are shown in Figure S6. Note that the theoretical feeding ratio of defective linkers is 41.7% (considering the seed layer). From the spectra, we can see that the doping levels of three defective linkers in SURMOF HKUST 1 are different (11.8, 12.7, and 39.1% for **M ip**, **M OH ip**, and **M pydc**; and 7.2, 7.7, and 33.3% for **A ip**, **A OH ip**, and **A pydc**, respectively), which correspond to the observation in $\Delta F - t$ growth curves. Another important information we can derive from the ^1H NMR spectra is that more defective linkers were incorporated in DE SURMOFs by the mixing method than by the alternating method. Compared to the defect engineered bulk samples, we find that a less amount of H_2ip was incorporated in DE SURMOFs,³⁰ while more amounts of $\text{H}_2\text{OH ip}$ and H_2pydc were integrated in the thin films by the mixing method.¹⁹

The measurements of ToF SIMS were also performed to determine the amount of defective and parent linkers in DE SURMOFs HKUST 1.⁴⁴ Unfortunately, it is difficult to

distinguish defective linkers ip and OH ip from the parent linker btc because of their close molecular structures and elemental compositions. SIMS is quite destructive due to the bombardment of the samples with 25 keV Bi³⁺ primary ions, thus yielding identical fragments for ip and btc, as ip can be seen as a btc substructure. Nevertheless, the situation for pydc is different, which can be distinguished from btc (Figure S7a). Finally, we find that the pydc concentration of pydc M is ~15% more than that of pydc A (Figure S7b) by referencing to precursor H₂pydc, which agrees with the results of NMR analysis.

3.3.2. UV-vis Spectroscopy. Since defects in the MOF framework may affect the electronic and optical properties of the material,^{33,45} UV-vis spectroscopy, shown in Figure 5, was

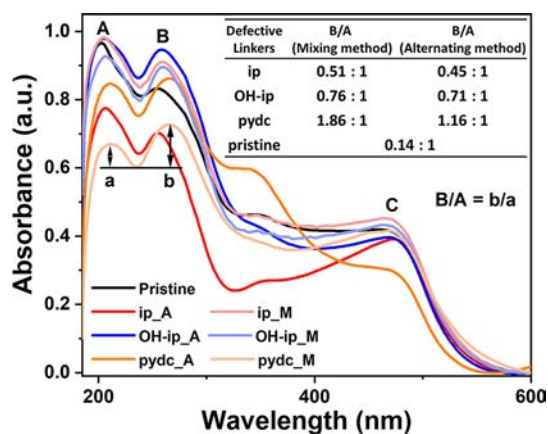


Figure 5. UV-vis spectra of pristine (black) and DE SURMOFs (color) HKUST 1. The inset table is the net absorption intensity ratio B/A of each spectrum.

employed to investigate the defects in DE SURMOFs HKUST 1. The UV-vis spectra show two characteristic absorption bands assigned to the π - π^* transition of the phenyl ring at about 205 nm (band A)^{46,47} and ligand to metal charge transfer at about 260 nm (band B).⁴⁸ Moreover, the absorption of d-d transitions in Cu paddlewheels can be observed in the visible range (around 460 nm, band C). As we can see in the spectra, by incorporating defective linkers, the intensity of band B increases relative to that of band A as compared to the pristine sample. In order to show how much the intensity of band B was increased more clearly, the ratio of the absorption intensities of bands B and A (B/A, shown in the inset table of Figure 5) is proposed. The B/A ratios reflect the defect density in DE SURMOF HKUST 1 and show an uptrend in the following sample order: defect linker free, ip defected, OH ip defected, and pydc defected. This tendency matches with the different doping levels of defective linkers and also with the electron donor/acceptor properties of functional groups at the fifth position of defective linkers.⁴⁹ Furthermore, the DE SURMOFs fabricated by the mixing method have larger B/A ratios than those synthesized by the alternating method. This means that more defects were incorporated in the framework by the mixing method, which is also supported by the ¹H NMR data.

3.3.3. Methanol Adsorption. The presence of metal and linker vacancies influences the porosity of DE SURMOF HKUST 1. Herein, methanol vapor adsorption was performed on SURMOFs to investigate the impact of defects on sorption properties, which are presented in Figure 6. The DE

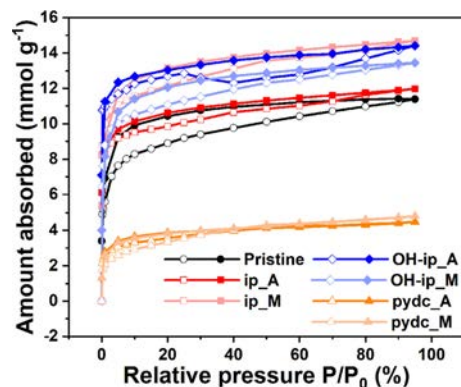


Figure 6. Methanol adsorption-desorption isotherms of pristine (black) and DE SURMOF HKUST 1 fabricated by the mixing method (light color) and alternating method (deep color).

SURMOFs HKUST 1 defected by H₂ip and H₂OH ip exhibit enhanced adsorption capacity in comparison with the parent one. Notably, ip M shows the highest methanol adsorption capacity (14.69 mmol g⁻¹) among all thin films. This result indicates that the porosity of DE SURMOF HKUST 1 is enhanced by incorporating defects in the lattice. On the contrary, the adsorption capacities of pydc M and pydc A are drastically reduced, which is probably due to the inclusion of large amounts of Cu(OAc)₂ in the pores of HKUST 1 through bonding with the pyridinic N of pydc. This situation differs from the reported bulk HKUST 1 defected by pydc, which shows a hysteresis/mesopore structure.¹⁹

3.3.4. SEM. The morphologies of DE SURMOFs were recorded by SEM, which are presented in Figure S8a. With the addition of different defective linkers, the obtained DE SURMOFs HKUST 1 show a diverse morphology compared to the pristine one. Moreover, the fabrication method influences the morphology. For DE SURMOFs defected by ip and OH ip, the samples fabricated by the mixing method are assembled by regular shaped and smooth octahedra or cubes, while those samples prepared by the alternating method show arbitrarily shaped MOF particles. However, the morphologies of pydc defected DE SURMOFs HKUST 1 seem independent from the synthetic method, with the SEM images of pydc M and pydc A doped HKUST 1 SURMOFs being similar. Moreover, the cross sectional SEM images of DE SURMOFs were measured (Figure S8b). The thickness of 10 cycles of the HKUST 1 seed layer is about 30 nm. The overall thicknesses of DE SURMOFs are also listed: about 110, 250, and 160 nm for ip M, OH ip M, and pydc M; and 100, 180, and 110 nm for ip A, OH ip A, and pydc A, respectively. Basically, the thickness of DE SURMOFs synthesized by the mixing method is thicker than that prepared by the alternating method, which agrees well with the total mass deposition of the two methods determined via QCM ($\Delta m_{\text{Mixing}} > \Delta m_{\text{Alternating}}$).

3.4. Comparison of Two Methods. For comparing the advantages of two methods, DE SURMOFs with higher density of ip were also fabricated. Specifically, ip M' with a feeding ratio of H₂ip:H₃btc = 2:1 and ip A' (ip A") with the repeating loop of 1 cycle of Cu(OAc)₂/H₃btc followed by 2 (4) cycles of the Cu(OAc)₂/defective linker were obtained. The $\Delta F - t$ growth curves are shown in Figure S9, from which we can see the growth of thin films. XRD patterns and methanol sorption isotherms (shown in Figures S10 and S11) confirm the phase purity and porosity of these DE SURMOFs

HKUST 1; however, the phase purity and porosity tend to decrease with the incorporation of more defect linkers in the framework.

Note that there are some flat stages appearing in the $\Delta F - t$ curves of **ip A'** and **ip A''** (Figure S12), which means that the surface of SURMOF is terminated and the growth of thin films is interrupted during the $\text{Cu}(\text{OAc})_2/\text{H}_2\text{ip}$ dosing steps.¹³ The growth of thin films could continue when alternating to dose $\text{Cu}(\text{OAc})_2/\text{H}_3\text{btc}$. Speculating from this observation and reasoning, the parent and defective linkers are obviously distributed in a layered "ABAB" fashion within DE SURMOFs. However, we are unable to provide rigorous proof of such a kind of defect distribution. That is to say, the alternating method probably offers a higher degree of controllability in the distribution of defects in DE SURMOFs HKUST 1. However, the mixing method is more efficient in incorporating defective linkers in SURMOF HKUST 1 compared to the alternating method. Furthermore, the samples **OH ip M** and **pydc M** exhibit higher defect densities than the corresponding bulk defect engineered HKUST 1 reference powder samples.¹⁹

4. CONCLUSIONS

In conclusion, two synthetic methods, mixing LBL method and alternating LBL method, are employed to fabricate DE SURMOFs HKUST 1 by partially substituting the parent H_3btc linker with defective linkers H_2ip , $\text{H}_2\text{OH ip}$, and H_2pydc . The frequency change against time ($\Delta F - t$) growth curves indicate the growth of DE SURMOFs HKUST 1. The measurements of XRD, IRRAS, and Raman spectroscopy confirm that the lattice of HKUST 1 remains intact with integrating defective linkers up to the reported doping levels. The defects in DE SURMOFs HKUST 1 were characterized by ^1H NMR, TOF SIMS, UV-vis, methanol vapor adsorption, and SEM. At last, we compared the advantages of two methods for incorporating defects in SURMOFs HKUST 1: the mixing method is more efficient to incorporate defects in the framework structure, while the alternating method shows a higher controllability in the distribution of these defects. These two methods supply a possible way to control the defect formation in MOF thin films.

AUTHOR INFORMATION

Corresponding Author

*E mail: roland.fischer@tum.de.

ORCID

Sebastian Henke: 0000 0003 1502 6038

Bernhard Rieger: 0000 0002 0023 884X

Roland A. Fischer: 0000 0002 7532 5286

Notes

The authors declare no competing financial interest.

ACKNOWLEDGMENTS

Z.W. is grateful to the China Scholarship Council (CSC).

REFERENCES

- (1) Furukawa, H.; Cordova, K. E.; O'Keeffe, M.; Yaghi, O. M. The Chemistry and Applications of Metal Organic Frameworks. *Science* **2013**, *341*, 1230444.
- (2) Li, H.; Eddaoudi, M.; O'Keeffe, M.; Yaghi, O. M. Design and Synthesis of an Exceptionally Stable and Highly Porous Metal Organic Framework. *Nature* **1999**, *402*, 276.
- (3) Zhou, H. C. J.; Kitagawa, S. Metal–Organic Frameworks (Mofs). *Chem. Soc. Rev.* **2014**, *43*, 5415–5418.
- (4) Murray, L. J.; Dinca, M.; Long, J. R. Hydrogen Storage in Metal–Organic Frameworks. *Chem. Soc. Rev.* **2009**, *38*, 1294–1314.
- (5) Li, J. R.; Sculley, J.; Zhou, H. C. Metal Organic Frameworks for Separations. *Chem. Rev.* **2012**, *112*, 869–932.
- (6) Chughtai, A. H.; Ahmad, N.; Younus, H. A.; Laypkov, A.; Verpoort, F. Metal–Organic Frameworks: Versatile Heterogeneous Catalysts for Efficient Catalytic Organic Transformations. *Chem. Soc. Rev.* **2015**, *44*, 6804–6849.
- (7) Kreno, L. E.; Leong, K.; Farha, O. K.; Allendorf, M.; Van Duyne, R. P.; Hupp, J. T. Metal Organic Framework Materials as Chemical Sensors. *Chem. Rev.* **2012**, *112*, 1105–1125.
- (8) Czaja, A. U.; Trukhan, N.; Müller, U. Industrial Applications of Metal Organic Frameworks. *Chem. Soc. Rev.* **2009**, *38*, 1284–1293.
- (9) Zhu, Q. L.; Xu, Q. Metal Organic Framework Composites. *Chem. Soc. Rev.* **2014**, *43*, 5468–5512.
- (10) Tanabe, K. K.; Cohen, S. M. Postsynthetic Modification of Metal Organic Frameworks—a Progress Report. *Chem. Soc. Rev.* **2011**, *40*, 498–519.
- (11) Dissegna, S.; Epp, K.; Heinz, W. R.; Kieslich, G.; Fischer, R. A. Defective Metal Organic Frameworks. *Adv. Mater.* **2018**, *30*, 1704501.
- (12) Fang, Z.; Bueken, B.; De Vos, D. E.; Fischer, R. A. Defect Engineered Metal Organic Frameworks. *Angew. Chem., Int. Ed.* **2015**, *54*, 7234–7254.
- (13) Wang, Z.; Wannapaiboon, S.; Rodewald, K.; Tu, M.; Rieger, B.; Fischer, R. A. Directing the Hetero Growth of Lattice Mismatched Surface Mounted Metal–Organic Frameworks by Functionalizing the Interface. *J. Mater. Chem. A* **2018**, *6*, 21295–21303.
- (14) Wannapaiboon, S.; Tu, M.; Fischer, R. A. Liquid Phase Heteroepitaxial Growth of Moisture Tolerant MOF 5 Isotype Thin Films and Assessment of the Sorption Properties by Quartz Crystal Microbalance. *Adv. Funct. Mater.* **2014**, *24*, 2696–2705.
- (15) Bétard, A.; Fischer, R. A. Metal Organic Framework Thin Films: From Fundamentals to Applications. *Chem. Rev.* **2012**, *112*, 1055–1083.
- (16) Zhang, Z.; Chen, Y.; Xu, X.; Zhang, J.; Xiang, G.; He, W.; Wang, X. Well Defined Metal Organic Framework Hollow Nanocages. *Angew. Chem., Int. Ed.* **2014**, *53*, 429–433.
- (17) Behrens, K.; Mondal, S. S.; Nöske, R.; Baburin, I. A.; Leoni, S.; Günter, C.; Weber, J.; Holdt, H. J. Microwave Assisted Synthesis of Defects Metal Imidazolate Amide Imidate Frameworks and Improved CO_2 Capture. *Inorg. Chem.* **2015**, *54*, 10073–10080.
- (18) Liu, Y.; Klet, R. C.; Hupp, J. T.; Farha, O. Probing the Correlations between the Defects in Metal Organic Frameworks and Their Catalytic Activity by an Epoxide Ring Opening Reaction. *Chem. Commun.* **2016**, *52*, 7806–7809.
- (19) Fang, Z.; Dürholt, J. P.; Kauer, M.; Zhang, W.; Lochenie, C.; Jee, B.; Albada, B.; Metzler Nolte, N.; Pöppel, A.; Weber, B.; Muhler, M.; Wang, Y.; Schmid, R.; Fischer, R. A. Structural Complexity in Metal Organic Frameworks: Simultaneous Modification of Open Metal Sites and Hierarchical Porosity by Systematic Doping with Defective Linkers. *J. Am. Chem. Soc.* **2014**, *136*, 9627–9636.
- (20) Stassen, I.; Burtch, N.; Talin, A.; Falcaro, P.; Allendorf, M.; Ameloot, R. An Updated Roadmap for the Integration of Metal Organic Frameworks with Electronic Devices and Chemical Sensors. *Chem. Soc. Rev.* **2017**, *46*, 3185–3241.

- (21) Babu, D. J.; He, G.; Hao, J.; Vahdat, M. T.; Schouwink, P. A.; Mensi, M.; Agrawal, K. V. Restricting Lattice Flexibility in Polycrystalline Metal Organic Framework Membranes for Carbon Capture. *Adv. Mater.* **2019**, *31*, 1900855.
- (22) Eum, K.; Hayashi, M.; De Mello, M. D.; Xue, F.; Kwon, H. T.; Tsapatsis, M. ZIF 8 Membrane Separation Performance Tuning by Vapor Phase Ligand Treatment. *Angew. Chem., Int. Ed.* **2019**, *58*, 16390–16394.
- (23) Hillman, F.; Brito, J.; Jeong, H. K. Rapid One Pot Microwave Synthesis of Mixed Linker Hybrid Zeolitic Imidazolate Framework Membranes for Tunable Gas Separations. *ACS Appl. Mater. Interfaces* **2018**, *10*, 5586–5593.
- (24) Hou, Q.; Wu, Y.; Zhou, S.; Wei, Y.; Caro, J.; Wang, H. Ultra Tuning of the Aperture Size in Stiffened ZIF 8 Cm Frameworks with Mixed Linker Strategy for Enhanced CO₂/CH₄ Separation. *Angew. Chem., Int. Ed.* **2019**, *58*, 327–331.
- (25) Lee, M. J.; Kwon, H. T.; Jeong, H. K. High Flux Zeolitic Imidazolate Framework Membranes for Propylene/Propane Separation by Postsynthetic Linker Exchange. *Angew. Chem., Int. Ed.* **2018**, *57*, 156–161.
- (26) Shimoni, R.; He, W.; Liberman, I.; Hod, I. Tuning of Redox Conductivity and Electrocatalytic Activity in Metal–Organic Framework Films Via Control of Defect Site Density. *J. Phys. Chem. C* **2019**, *123*, 5531–5539.
- (27) Vermoortele, F.; Bueken, B.; Le Bars, G.; Van de Voorde, B.; Vandichel, M.; Houthoofd, K.; Vimont, A.; Daturi, M.; Waroquier, M.; Van Speybroeck, V.; Kirschhock, C.; De Vos, D. E. Synthesis Modulation as a Tool to Increase the Catalytic Activity of Metal Organic Frameworks: The Unique Case of Uio 66(Zr). *J. Am. Chem. Soc.* **2013**, *135*, 11465–11468.
- (28) Vermoortele, F.; Ameloot, R.; Alaerts, L.; Matthesen, R.; Carlier, B.; Fernandez, E. V. R.; Gascon, J.; Kapteijn, F.; De Vos, D. E. Tuning the Catalytic Performance of Metal–Organic Frameworks in Fine Chemistry by Active Site Engineering. *J. Mater. Chem.* **2012**, *22*, 10313–10321.
- (29) St Petkov, P.; Vayssilov, G. N.; Liu, J.; Shekhah, O.; Wang, Y.; Wöll, C.; Heine, T. Defects in Mofs: A Thorough Characterization. *ChemPhysChem* **2012**, *13*, 2025–2029.
- (30) Zhang, W.; Kauer, M.; Guo, P.; Kunze, S.; Cwik, S.; Muhler, M.; Wang, Y.; Epp, K.; Kieslich, G.; Fischer, R. A. Impact of Synthesis Parameters on the Formation of Defects in HKUST 1. *Eur. J. Inorg. Chem.* **2017**, *2017*, 925–931.
- (31) Barin, G.; Krungleviciute, V.; Gutov, O.; Hupp, J. T.; Yildirim, T.; Farha, O. K. Defect Creation by Linker Fragmentation in Metal–Organic Frameworks and Its Effects on Gas Uptake Properties. *Inorg. Chem.* **2014**, *53*, 6914–6919.
- (32) Svane, K. L.; Bristow, J. K.; Gale, J. D.; Walsh, A. Vacancy Defect Configurations in the Metal Organic Framework Uio 66: Energetics and Electronic Structure. *J. Mater. Chem. A* **2018**, *6*, 8507–8513.
- (33) Müller, K.; Singh Malhi, J.; Wohlgemuth, J.; Fischer, R. A.; Wöll, C.; Gliemann, H.; Heinke, L. Water as a Modulator in the Synthesis of Surface Mounted Metal Organic Framework Films of Type HKUST 1. *Dalton Trans.* **2018**, *47*, 16474–16479.
- (34) Li, W.; Zhang, Y.; Zhang, C.; Meng, Q.; Xu, Z.; Su, P.; Li, Q.; Shen, C.; Fan, Z.; Qin, L.; Zhang, G. Transformation of Metal Organic Frameworks for Molecular Sieving Membranes. *Nat. Commun.* **2016**, *7*, 11315.
- (35) Shekhah, O.; Wang, H.; Kowarik, S.; Schreiber, F.; Paulus, M.; Tolan, M.; Sternemann, C.; Evers, F.; Zacher, D.; Fischer, R. A.; Wöll, C. Step by Step Route for the Synthesis of Metal Organic Frameworks. *J. Am. Chem. Soc.* **2007**, *129*, 15118–15119.
- (36) Shekhah, O.; Wang, H.; Zacher, D.; Fischer, R. A.; Wöll, C. Growth Mechanism of Metal–Organic Frameworks: Insights into the Nucleation by Employing a Step by Step Route. *Angew. Chem., Int. Ed.* **2009**, *48*, 5038–5041.
- (37) Tu, M.; Wannapaiboon, S.; Fischer, R. A. Liquid Phase Stepwise Growth of Surface Mounted Metal–Organic Frameworks for Exploratory Research and Development of Applications. *Inorg. Chem. Front.* **2014**, *1*, 442–463.
- (38) Stavila, V.; Volponi, J.; Katzenmeyer, A. M.; Dixon, M. C.; Allendorf, M. D. Kinetics and Mechanism of Metal–Organic Framework Thin Film Growth: Systematic Investigation of HKUST 1 Deposition on QCM Electrodes. *Chem. Sci.* **2012**, *3*, 1531–1540.
- (39) Cheetham, A. K.; Bennett, T. D.; Coudert, F. X.; Goodwin, A. L. Defects and Disorder in Metal Organic Frameworks. *Dalton Trans.* **2016**, *45*, 4113–4126.
- (40) Delen, G.; Ristanović, Z.; Mandemaker, L. D. B.; Weckhuysen, B. M. Mechanistic Insights into Growth of Surface Mounted Metal Organic Framework Films Resolved by Infrared (Nano) Spectroscopy. *Chem. – Eur. J.* **2018**, *24*, 187–195.
- (41) Todaro, M.; Alessi, A.; Sciortino, L.; Agnello, S.; Cannas, M.; Gelardi, F. M.; Buscarino, G. Investigation by Raman Spectroscopy of the Decomposition Process of HKUST 1 Upon Exposure to Air. *J. Spectrosc.* **2016**, *2016*, 1–7.
- (42) Zhang, W.; Kauer, M.; Halbherr, O.; Epp, K.; Guo, P.; Gonzalez, M. L.; Xiao, D. J.; Wiktor, C.; Llabrés i Xamena, F. X.; Wöll, C.; Wang, Y.; Muhler, M.; Fischer, R. A. Rutheniummetal–Organic Frameworks with Different Defect Types: Influence on Porosity, Sorption, and Catalytic Properties. *Chem. – Eur. J.* **2016**, *22*, 14297–14307.
- (43) Sholl, D. S.; Lively, R. P. Defects in Metal Organic Frameworks: Challenge or Opportunity? *J. Phys. Chem. Lett.* **2015**, *6*, 3437–3444.
- (44) Ladnorg, T.; Welle, A.; Heißler, S.; Wöll, C.; Gliemann, H. Site Selective Growth of Surface Anchored Metal Organic Frameworks on Self Assembled Monolayer Patterns Prepared by AFM Nanografting. *Beilstein J. Nanotechnol.* **2013**, *4*, 638–648.
- (45) Müller, K.; Fink, K.; Schöttner, L.; Koenig, M.; Heinke, L.; Wöll, C. Defects as Color Centers: The Apparent Color of Metal Organic Frameworks Containing Cu²⁺ Based Paddle Wheel Units. *ACS Appl. Mater. Interfaces* **2017**, *9*, 37463–37467.
- (46) Mahalakshmi, G.; Balachandran, V. FT IR and FT Raman Spectra, Normal Coordinate Analysis and Ab Initio Computations of Trimesic Acid. *Spectrochim. Acta A* **2014**, *124*, 535–547.
- (47) Kania, R.; Malongwe, J. K. E.; Nachtigallová, D.; Krausko, J.; Gladich, I.; Roeselová, M.; Heger, D.; Klán, P. Spectroscopic Properties of Benzene at the Air–Ice Interface: A Combined Experimental–Computational Approach. *J. Phys. Chem. A* **2014**, *118*, 7535–7547.
- (48) Gu, Z. G.; Heinke, L.; Wöll, C.; Neumann, T.; Wenzel, W.; Li, Q.; Fink, K.; Gordan, O. D.; Zahn, D. R. T. Experimental and Theoretical Investigations of the Electronic Band Structure of Metal Organic Frameworks of HKUST 1 Type. *Appl. Phys. Lett.* **2015**, *107*, 183301.
- (49) Nazeeruddin, M. K.; Zakeeruddin, S. M.; Kalyanasundaram, K. Enhanced Intensities of the Ligand to Metal Charge Transfer Transitions in Ru(III) and Os(III) Complexes of Substituted Bipyridines. *J. Phys. Chem.* **1993**, *97*, 9607–9612.

Repository KITopen

Dies ist ein Postprint/begutachtetes Manuskript.

Empfohlene Zitierung:

Wang, Z.; Henke, S.; Paulus, M.; Welle, A.; Fan, Z.; Rodewald, K.; Rieger, B.; Fischer, R. A. [Defect Creation in Surface-Mounted Metal–Organic Framework Thin Films.](#) 2020. ACS applied materials & interfaces, 12. doi: [10.5445/IR/1000104558](https://doi.org/10.5445/IR/1000104558)

Zitierung der Originalveröffentlichung:

Wang, Z.; Henke, S.; Paulus, M.; Welle, A.; Fan, Z.; Rodewald, K.; Rieger, B.; Fischer, R. A. [Defect Creation in Surface-Mounted Metal–Organic Framework Thin Films.](#) 2020. ACS applied materials & interfaces, 12 (2), 2655–2661. doi: [10.1021/acsami.9b18672](https://doi.org/10.1021/acsami.9b18672)

Lizenzinformationen: [KITopen-Lizenz](#)